

# Towards Calibrated Robust Fine-Tuning of Vision-Language Models

Changdae Oh\*<sup>1</sup> Hyesu Lim\*<sup>2</sup> Mijoo Kim<sup>3</sup> Jaegul Choo<sup>2</sup> Alexander Hauptmann<sup>4</sup> Zhi-Qi Cheng<sup>4</sup>  
Kyungwoo Song<sup>5</sup>

## Abstract

Robust fine-tuning aims to ensure performance on out-of-distribution (OOD) samples, which is sometimes compromised by pursuing adaptation on in-distribution (ID) samples. However, another criterion for reliable machine learning – *confidence calibration* has been overlooked despite its increasing demand for real-world high-stakes applications, e.g., autonomous driving. We raise concerns about the calibration of fine-tuned vision-language models (VLMs) under distribution shift by showing that naive fine-tuning and even state-of-the-art robust fine-tuning hurt the calibration of pre-trained VLMs, especially on OOD datasets. We first show the OOD calibration error is bounded from above with ID calibration errors and domain discrepancy between ID and OOD. From this analysis, we propose **CaRot**, a calibrated robust fine-tuning method that incentivizes ID calibration and robust prediction across domains to reduce the upper bound of OOD calibration error. Extensive experiments on three types of distribution shifts (natural, synthetic, and adversarial) on ImageNet-1K classification demonstrate the effectiveness of CaRot across diverse environments. We justify the empirical success of CaRot through our theoretical analysis. Our code is available here<sup>1</sup>.

## 1. Introduction

Robust fine-tuning community points out conventional fine-tuning methods compromise the generalization ability of foundation models (Bommasani et al., 2021) and suggests

\*Equal contribution <sup>1</sup>University of Seoul, Seoul, South Korea <sup>2</sup>KAIST AI, Seongnam-si, South Korea <sup>3</sup>Chung-Ang University, Seoul, South Korea <sup>4</sup>Carnegie Mellon University, Pittsburgh, PA, USA <sup>5</sup>Yonsei University, Seoul, South Korea. Correspondence to: Zhi-Qi Cheng <zhiqic@andrew.cmu.edu>, Kyungwoo Song <kyungwoo.song@yonsei.ac.kr>.

<sup>1</sup><https://anonymous.4open.science/r/CaRot-5C50>

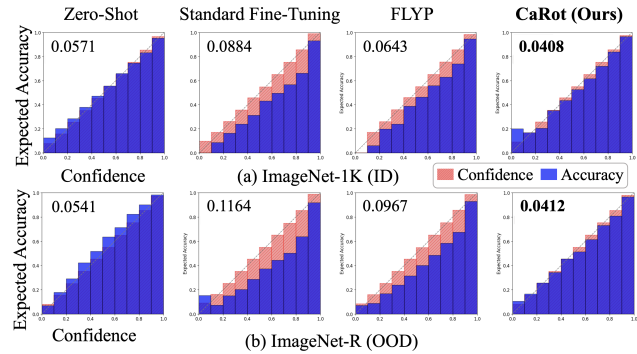


Figure 1: Reliability diagram (Niculescu-Mizil & Caruana, 2005) with expected calibration error (ECE) of zero-shot and fine-tuned (on ImageNet-1K) CLIP evaluated on ImageNet-1K (top) and ImageNet-R (bottom).

methods that aim to achieve good performance on data from both in-distribution (ID) and out-of-distribution (OOD). After Wortsman et al. (2022) and Kumar et al. (2022) amplified the discussion on the robustness of recent VLMs under distribution shifts, a wide range of research has followed (Lee et al., 2023; Goyal et al., 2023; Lee et al., 2023; Tian et al., 2023a; Oh et al., 2023).

However, ongoing studies on robust fine-tuning have focused only on accurate prediction, while neglecting *confidence calibration* (Murphy, 1972; DeGroot & Fienberg, 1983) (that represents how close the confidence of our predictor is to the actual correctness of predictions), which is another important criterion in reliable machine learning (ML). For example, it is crucial to avoid making incorrect predictions with high confidence in real-world decision-making systems, especially in high-stakes tasks such as autonomous driving and healthcare applications. After a seminal work (Guo et al., 2017) revealed the miscalibration problem of high-performing neural networks, a plethora of attempts followed to improve the calibration of neural network models through post-hoc adjustments (Zadrozny & Elkan, 2002; Guo et al., 2017; Kull et al., 2019; Zhang et al., 2020; Gupta et al., 2020) or train-time regularizations (Zhang et al., 2017; Sensoy et al., 2018; Thulasidasan et al., 2019; Müller et al., 2019; Mukhoti et al., 2020).

Recently, Minderer et al. (2021) systematically reviewed the

calibration of modern vision models across different model architectures, model sizes, and amounts of pre-training, and LeVine et al. (2023) inspected on the calibration of a zero-shot VLM (e.g., CLIP). However, to the best of our knowledge, no existing work addresses the calibration under distribution during fine-tuning of VLMs, which is timely to be investigated. In this work, we first inspect the calibration of fine-tuned VLMs under distribution shifts. As shown in Figure 1, existing fine-tuning methods (even the state-of-the-art fine-tuning method) hurt the confidence calibration in terms of expected calibration error (ECE; Naeini et al. (2015)) on ID and especially on OOD data. While there are several representative calibration methods, such as temperature scaling (Guo et al., 2017) and label smoothing (Szegedy et al., 2016), they work by decreasing (or increasing) the confidence of a model in an input-independent manner, and not carefully pursuing the desired confidence for each sample. Moreover, these methods basically do not consider distribution shifts, thus they cannot promise a good calibration on the OOD examples.

Having a goal to achieve good calibration under distribution shift, we derive a bound for OOD calibration error and show that it is bounded from above with ID calibration and divergence between ID and OOD domains. In addition, we further connect that bound with the OOD generalization error. Motivated by these theoretical analyses, we propose a calibrated robust fine-tuning **CaRot**. First, we recognize the divergence between ID and OOD domains can be reduced by achieving robust prediction against distribution shifts, so we adopt contrastive loss as our base learning objective with an expectation of its contribution to OOD robustness (Goyal et al., 2023). Second, we leverage input-dependent label smoothing obtained by self-distillation with an exponential moving average (EMA) teacher model for improving ID calibration as well as OOD robustness. During the early stage, our fine-tuning model consumes (pseudo) soft labels derived from the pre-trained model that act as informative prior distributions for the co-occurrence probability among in-batch samples. Here, these priors guide a contrastive learner to produce a calibrated prediction as a form of input-dependent label smoothing regularizer. As training goes on, the teacher model gradually acquires specific knowledge of the downstream dataset by performing EMA updates, so that it provides updated priors tailored to the ID domain. Eventually, OOD robustness and ID calibration endowed by the above two components contribute to improving OOD calibration (and also generalization).

We conduct extensive experiments of fine-tuning CLIP (Radford et al., 2021) on ImageNet-1K (Deng et al., 2009) classification task under three types of distribution shifts, including natural shift (ImageNet-V2/R/A/Sketch and ObjectNet), synthetic shift (ImageNet-C), and adversarial attack. By observing significant improvement in terms of expected cal-

ibration error on ID/OOD datasets as well as accuracy, we demonstrate the effectiveness of leveraging self-distillation with contrastive learning for robust calibration and adaptation.

**Contributions.** 1) We observe that the standard fine-tuning (even the state-of-the-art method) largely harms the calibration of pre-trained VLMs, especially OOD domains. 2) We provide a theoretical analysis for calibration and classification errors on OOD domains, and show that they are both bounded from above by ID calibration error and domain discrepancy. 3) Based on our theoretical results, we devise a calibrated robust fine-tuning method, CaRot, that adopts contrastive learning with self-distillation to pursue ID calibration and reduce domain discrepancy. 4) We demonstrate the efficacy of CaRot via extensive evaluations on ImageNet-1K distribution shifts, including natural shift, synthetic shift, and adversarial attack in terms of accuracy and calibration error on ID and OOD domains. The empirical success of CaRot is further explained by our theoretical framework.

## 2. Background and Related Work

### 2.1. Robust fine-tuning of visual foundation models

**Background.** Robust fine-tuning aims to achieve consistently high performance on both training (ID) and related but different test distributions (OOD). For validation, we commonly consider a covariate shift scenario for the classification task, where both ID and OOD domains share the class categories ( $\mathcal{Y}_{ID} = \mathcal{Y}_{OOD}$ ) and have the same conditional distribution  $P(Y|X)$ , but have different marginal distributions over input  $X$ . That is,  $P_{ID}(X) \neq P_{OOD}(X)$  but  $P_{ID}(Y|X) = P_{OOD}(Y|X)$ . Here, we evaluate the robustness of a model, which is fine-tuned on a training split of ID domain, on a test split of ID and that of OOD domains.

Beyond the ID generalization, there are a lot of works aiming at improving the generalization of fine-tuned models on the OOD domain. Wortsman et al. (2022) suggests using linearly interpolated model weight before and after fine-tuning to improve the robustness. Kumar et al. (2022) argued that first training the linear classification head upon the frozen feature extractor and then training the entire model improves the robustness rather than simultaneously training the feature extractor and classification head from the beginning. Lee et al. (2023) provided a method that selectively updates a subset of layers based on to cope with different kinds of distribution shifts. Meanwhile, Goyal et al. (2023) proposed to align the learning objective in fine-tuning with the pre-training stage by using contrastive loss instead of cross-entropy loss to preserve the robustness while pursuing adaptation. There is also a line of works that enforces soft constraints during parameter update via projection (Tian et al., 2023a;b). Although the above methods have provided

insights into the OOD generalization of foundation models, none of them consider confidence calibration, which is crucial for reliable ML applications. We investigate the calibration of fine-tuned CLIP and provide a method to achieve good ID and OOD calibration for the first time.

## 2.2. Confidence calibration

**Background.** The goal of confidence calibration is to match the softmax probabilities outputted for different inputs to the expected accuracy on these inputs. In a  $K$ -way classification setting, let  $X \in \mathbb{R}^d$  and  $Y \in \{1, \dots, K\}$  be random variables indicating inputs and labels, respectively. A dataset with  $N$  independent samples from the joint distribution  $P(X, Y) = P(Y|X)P(X)$  is denoted by  $\{(x_n, y_n)\}_{n=1}^N$ . Let  $f$  be a classifier and  $f(y|x) = \hat{p}$  be a confidence, i.e., the maximum of output probability corresponding to its prediction  $\hat{y}$ . We say a model is *perfectly-calibrated* when  $\mathbb{P}(\hat{y} = y | \hat{p} = p) = p, \forall p \in [0, 1]$ . To measure the calibration of a model, the expected calibration error (ECE; Naeini et al. (2015)) can be derived as  $\mathbb{E}[|\mathbb{P}(\hat{y} = y | \hat{p} = p) - p|]$ . In practice, we use an empirical ECE as an approximation of the calibration error, which divides  $N$  confidence scores into  $M$  uniform confidence bins  $\{\text{bin}_m\}_{m=1}^M$  and takes a weighted average of the gap between accuracy (acc) and confidence (conf) of each bin, i.e.  $\text{ECE} = \sum_{m=1}^M \frac{|\text{bin}_m|}{N} |\text{acc}(\text{bin}_m) - \text{conf}(\text{bin}_m)|$ .

After some early research on calibrated prediction (Murphy, 1972; DeGroot & Fienberg, 1983), lots of follow-up studies have been conducted. As a seminal work, Guo et al. (2017) revealed the miscalibration problem of neural networks, then, Minderer et al. (2021) provided a comprehensive analysis on the calibration of modern vision models with consideration on distribution shift, and recently LeVine et al. (2023) investigated calibration of the zero-shot vision-language model. To improve the calibration of predictive models, Temperature Scaling (TS; Guo et al. (2017)) and Label Smoothing (LS; Szegedy et al. (2016)) are two representative lines of works. While the standard TS seeks a single parameter called temperature  $\tau$  to adjust the probability output on the single ID dataset, Gong et al. (2021) provides a method for learning multiple temperatures leveraging multiple sources of ID domains, and Yu et al. (2022) propose a method for learning a regressor to produce input-dependent temperature over multiple ID domains. Joy et al. (2023) likewise provides an input-dependent temperature scaling method that trains an auxiliary predictor adopting variational autoencoder (Kingma & Welling, 2013).

Meanwhile, it is shown that LS (Szegedy et al., 2016) can be helpful not only for generalization but for calibration (Müller et al., 2019; Thulasidasan et al., 2019). The standard LS endows uniform prior distribution over the output probability of models, but there are many attempts to induce

more informative priors by adopting Mixup (Thulasidasan et al., 2019), pre-trained model (Guo et al., 2021), and aggregated predictions of models (Zhang & Sabuncu, 2020; Zhang et al., 2021). Besides, there are some interpretations of knowledge distillation as an input-dependent LS (Yuan et al., 2020; Zhang & Sabuncu, 2020). In detail, Zhang & Sabuncu (2020) provides a new perspective of self-distillation (having a previous self as a teacher model) as an amortized maximum a posterior (MAP) method.

However, existing approaches do not consider distribution shift (Zhang & Sabuncu, 2020), assume accessibility to target domain (Gong et al., 2021; Yu et al., 2022), assume specific type of distribution shift (Tomani et al., 2021), cannot adjust confidences individually (Guo et al., 2017; Szegedy et al., 2016), or require additional model (Joy et al., 2023). In this work, we advocate the use of EMA self-distillation to improve ID calibration and OOD robustness.

## 3. Theoretical Analysis on OOD Calibration and Generalization

To improve OOD calibration of models with only access to ID data, we first identify the factors that affect OOD calibration. For this, we take inspiration from the domain adaptation literature (Ben-David et al., 2010; Zhao et al., 2018; Yu et al., 2022) to derive a similar bound for the distribution shift scenario and tailor it to calibration setup.

Let  $\mathcal{D}$  be a domain on input space  $\mathcal{X}$  and  $\mathcal{Y} = \{0, 1\}$  as a label space for the binary classification. Here, we define  $h_0(\cdot) : \mathcal{X} \rightarrow [0, 1]$  as a desired calibrated predictor for label  $y$ , which minimizes the calibration error (Murphy, 1972)  $\mathbb{E}_{x \sim \mathcal{D}}[|h(x) - c(x)|^2]$  where  $c(x) = \mathbb{E}_y[y|h(x)]$  is the expected value of  $y$  given a confidence level  $h(x)$ . That is, the  $h_0$  always produces the calibrated prediction for  $y$  given  $x$  so that the output confidence  $h_0(x)$  matches the expectation of  $y$  over the subset of samples that have the same confidence as  $h_0(x)$ . Our goal is to learn a hypothesis function  $h : \mathcal{X} \rightarrow [0, 1]$  as a robust predictor that outputs reliable probability on samples from the unseen OOD domain defined by a distribution  $\mathcal{D}_{\text{OOD}}$  as well as the ID domain  $\mathcal{D}_{\text{ID}}$  where the predictor is trained on, such that the error  $\varepsilon_{\mathcal{D}}(h) = \mathbb{E}_{x \sim \mathcal{D}}[|h_0(x) - h(x)|]$  is small for two different domains  $\mathcal{D} \in \{\mathcal{D}_{\text{ID}}, \mathcal{D}_{\text{OOD}}\}$ . We assume the covariate shift scenario (§ 2) that only the marginal distribution over  $\mathcal{X}$  is changed while the distribution over  $\mathcal{Y}$  is preserved as  $P_y$ .

Before going further, we need a distance measure between two distributions  $\mathcal{D}_{\text{ID}}$  and  $\mathcal{D}_{\text{OOD}}$ . We adopt  $\mathcal{H}$ -divergence (Ben-David et al., 2010) as a distance measure, which can be regarded as a practical relaxation of total variation distance.

**Definition 3.1** ( $\mathcal{H}$ -divergence). *Let  $\mathcal{H}$  be a hypothesis class for input space  $\mathcal{X}$  and a collection of subsets from  $\mathcal{X}$  is denoted by  $\mathcal{A}_{\mathcal{H}} := \{h^{-1}(1) | h \in \mathcal{H}\}$  which is the support*



of hypothesis  $h \in \mathcal{H}$ . The  $\mathcal{H}$ -divergence between two distributions  $\mathcal{D}$  and  $\mathcal{D}'$  is  $d_{\mathcal{H}}(\mathcal{D}, \mathcal{D}') = 2 \sup_{A \in \mathcal{A}_{\mathcal{H}}} |\mathbb{P}_{\mathcal{D}}(A) - \mathbb{P}_{\mathcal{D}'}(A)|$ .

The above definition is particularly attractive because it allows us to indirectly reflect the model’s predictions in our measure of the distance between distributions. Next, we define the optimal hypothesis  $h^*$ , which minimizes the combination error on both ID and OOD domain, i.e.,  $h^* := \arg \min_{h \in \mathcal{H}} \varepsilon_{\mathcal{D}_{\text{ID}}}(h) + \varepsilon_{\mathcal{D}_{\text{OOD}}}(h)$ , and let  $\Delta$  denote the optimal joint error  $\Delta := \varepsilon_{\mathcal{D}_{\text{ID}}}(h^*) + \varepsilon_{\mathcal{D}_{\text{OOD}}}(h^*)$ . In addition, we further analyze the OOD classification error under the same framework by leveraging the decomposition of classification error (Murphy, 1972; Park et al., 2020):

$$\underbrace{\mathbb{E}[|h(x) - y|^2]}_{\text{classification error}} = \underbrace{\mathbb{E}[|h(x) - c(x)|^2]}_{\text{calibration error}} + 1 - \underbrace{\mathbb{E}[|c(x)|^2]}_{\text{sharpness}}$$

where  $\mathbb{E}[|h(x) - y|^2]$  is an expected mean-squared classification error and  $\mathbb{E}[|c(x)|^2]$  denotes the *sharpness* (Sanders, 1963) term rewarding the predictor  $h(\cdot)$  which produces outputs towards zero or one.

Now, we first derive an upper bound for the calibration error. Then, by plugging the above equation into that bound, we obtain another upper bound for the classification error.

**Theorem 3.2.** *Let  $h : \mathcal{X} \rightarrow [0, 1]$  be a real-valued function in a hypothesis class  $\mathcal{H}$  with a pseudo dimension  $\mathcal{Pdim}(\mathcal{H}) = d$ . If  $\hat{\mathcal{D}}_{\text{ID}}$  and  $\hat{\mathcal{D}}_{\text{OOD}}$  are the empirical distribution constructed by  $n$ -size i.i.d. samples, drawn from  $\mathcal{D}_{\text{ID}}$  and  $\mathcal{D}_{\text{OOD}}$  respectively, then for any  $\delta \in (0, 1)$ , and for all  $h$ , two bounds below hold with probability at least  $1 - \delta$ .*

$$\begin{aligned} \text{i) } \varepsilon_{\mathcal{D}_{\text{OOD}}}(h) &\leq \varepsilon_{\hat{\mathcal{D}}_{\text{ID}}}(h) + \frac{1}{2} d_{\bar{\mathcal{H}}}(\hat{\mathcal{D}}_{\text{ID}}, \hat{\mathcal{D}}_{\text{OOD}}) \\ &\quad + \Delta + \mathcal{O}\left(\sqrt{\frac{d \log(n/d) + \log(1/\delta)}{n}}\right) \\ \text{ii) } \mathbb{E}_{\mathcal{D}_{\text{OOD}}} [|h(x) - y|^2] + \mathbb{E}_{\mathcal{D}_{\text{OOD}}} [|c(x)|^2] &\leq \varepsilon_{\hat{\mathcal{D}}_{\text{ID}}}(h) \\ &\quad + \frac{1}{2} d_{\bar{\mathcal{H}}}(\hat{\mathcal{D}}_{\text{ID}}, \hat{\mathcal{D}}_{\text{OOD}}) + \Delta + \mathcal{O}\left(\sqrt{\frac{d \log(n/d) + \log(1/\delta)}{n}}\right) \end{aligned}$$

where  $\bar{\mathcal{H}} := \{\text{sign}(|h(x) - h'(x)| - t) | h, h' \in \mathcal{H}, 0 \leq t \leq 1\}$ . Here we note that the first and second terms of RHS in both bounds indicate the empirical ID domain calibration error and  $\mathcal{H}$ -divergence between ID and OOD domains. From the first inequality, we can see that minimizing ID calibration error and  $\mathcal{H}$ -divergence between two domains can reduce the upper bound of OOD calibration error. Moreover, they also contribute to reducing the upper bound for the summation of classification error and the sharpness of prediction over the OOD domain. In essence, we can reduce both OOD calibration and classification errors by reducing ID calibration error and divergence (recognized by a classifier  $h$ ) between ID and OOD domains.

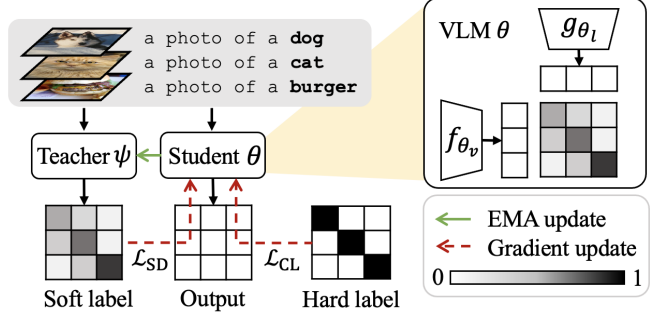


Figure 2: CaRot overview. We use contrastive loss with hard label as  $\mathcal{L}_{\text{CL}}$  (Eq. 1) and self-distillation that uses teacher output as a soft label as  $\mathcal{L}_{\text{SD}}$  (Eq. 2) to update the student model  $\theta$ . We update teacher model  $\psi$  using EMA update. Darker and lighter elements denote values closer to 1 and 0, respectively. Both teacher and student models share identical VLM architecture consisting of image  $f_{\theta_v}$  and text  $g_{\theta_t}$  encoders. Given (image, text) pair data, the model outputs the similarity map across encoded representations.

## 4. Methods

Our goal is to achieve good performance on the tuned ID domain while not hurting the already possessing generalization ability. At the same time, we hope the model outputs calibrated predictions for both ID and OOD domains. Motivated by our analysis of OOD calibration and generalization in § 3, we propose a calibrated robust fine-tuning method that improves ID calibration and pursues robustness that closes the distance between classifier predictions over ID and OOD domains (that contributes to reduce  $\mathcal{H}$ -divergence). First, we adopt contrastive loss, which is known to be effective in preserving the strong robustness of a zero-shot model (Goyal et al., 2023). Then, to enforce calibrated predictions as well as robustness, we employ self-distillation as an input-dependent label smoothing (Zhang & Sabuncu, 2020). Following previous works (Wortsman et al., 2022; Kumar et al., 2022; Goyal et al., 2023), we set CLIP as our target VLM. An overview of our methods is illustrated in Figure 2.

### 4.1. Contrastive learning for fine-tuning

Goyal et al. (2023) emphasizes that aligning the learning objective in fine-tuning and pre-training time (FLYP; fine-tune like you pre-train) is crucial to improve the robustness of the fine-tuned model under distribution shifts. Following FLYP, we employ contrastive learning as our base learning objective for CLIP fine-tuning.

CLIP consists of image encoder  $f_{\theta_v}(\cdot)$  and text encoder  $g_{\theta_t}(\cdot)$ . Each encoder produces  $L_2$ -normalized representation to compute the similarity between image and text. Given a downstream minibatch of  $B$  (image, text) pairs

Table 1: Natural shift results. ID indicates IN-1K and OOD indicates the average result of five natural shift variants.

Method	Acc. ( $\uparrow$ )		ECE ( $\downarrow$ ) w/o TS		ECE ( $\downarrow$ ) w/ TS	
	ID	OOD	ID	OOD	ID	OOD
ZS	0.6832	0.5840	0.0571	0.0737	0.0392	0.1217
	<i>w/o ensemble</i>					
FT	0.8153	0.5750	0.0884	0.2186	0.0463	0.1259
LP-FT	0.8217	0.5822	0.0696	0.1936	<b>0.0382</b>	0.0979
FLYP	0.8258	0.5946	0.0643	0.1831	0.0392	0.1217
<b>CaRot</b>	<b>0.8337</b>	<b>0.6222</b>	<b>0.0408</b>	<b>0.0916</b>	0.0397	<b>0.0941</b>
	<i>w/ ensemble (WiSE-FT <math>\alpha_{ensemble} = 0.5</math>)</i>					
FT	0.8043	0.6350	0.2129	0.1764	<b>0.0423</b>	0.0904
LP-FT	<b>0.8197</b>	0.6003	0.1921	0.1651	0.0754	0.1276
FLYP	0.8102	0.6423	0.0794	0.1327	0.0441	0.0856
<b>CaRot</b>	0.8040	<b>0.6443</b>	<b>0.0453</b>	<b>0.0759</b>	0.0453	<b>0.0774</b>

$\mathcal{B} = \{(I_i, T_i)\}_{i=1}^B$ , contrastive loss can be written as

$$\mathcal{L}_{CL}(\mathcal{B}, \theta) := \sum_{i=1}^B -\log \frac{\exp(f_{\theta_v}(I_i) \cdot g_{\theta_t}(T_i))}{\sum_{j=1}^B \exp(f_{\theta_v}(I_i) \cdot g_{\theta_t}(T_j))} + \sum_{i=1}^B -\log \frac{\exp(f_{\theta_v}(I_i) \cdot g_{\theta_t}(T_i))}{\sum_{j=1}^B \exp(f_{\theta_v}(I_j) \cdot g_{\theta_t}(T_i))}, \quad (1)$$

where  $\theta = \{\theta_v, \theta_t\}$  are the parameters of image and text encoders. Both image and text encoders are updated during fine-tuning as done in the pre-train phase, and we use OpenAI templates (Radford et al., 2021) to create (image, text) pairs from the image classification dataset that consists of (image, class) pairs.

## 4.2. Self-distillation as an input-dependent LS

To enforce good calibration during fine-tuning, we take a look at the label smoothing (LS) as a train-time calibration regularizer. While the standard form of LS always produces a fixed soft label regardless of the input data (enforcing uniform prior over prediction), one may want to alternatively design soft labels considering the variation of data instances. By witnessing the importance of a calibration method’s expressivity and confidence diversity (Zhang et al., 2020; Zhang & Sabuncu, 2020), we consider an input-dependent approach that accounts for the uncertainty (i.e., a desired confidence) associated with each input. For example, classifying a dog image from images of car or airplane could be less challenging than classifying it from images of cat or wolf. Ideally, a calibrated model would output higher confidence for the former than the latter case. To produce soft labels that reflect this kind of data similarity structure, we leverage the outputs of the (pre-)trained model as input-dependent priors, as is done in the field of knowledge distillation (Yuan et al., 2020; Zhang et al., 2021; Zhang & Sabuncu, 2020).

We first initialize both teacher and student networks with a pre-trained CLIP model (including both image and text

Table 2: Synthetic shift. mCE is mean corruption error.

Method	mCE ( $\downarrow$ )	ECE ( $\downarrow$ )	mCE ( $\downarrow$ )	ECE ( $\downarrow$ )
ZS	0.6554	0.0621	0.6554	0.0621
	<i>w/o ensemble</i>		<i>w/ ensemble</i>	
FT	0.5514	0.2034	0.5054	0.1353
LP-FT	0.5381	0.1750	0.5686	0.3704
FLYP	0.5245	0.1698	<b>0.4965</b>	0.1107
<b>CaRot</b>	<b>0.4936</b>	<b>0.1054</b>	0.4964	<b>0.0969</b>

encoders), and then, update the student model using gradient descent for every iteration, while slowly updating the teacher model that has  $\psi = \{\psi_v, \psi_t\}$  as parameters using exponential moving average (EMA) with momentum of  $\alpha$  at every  $t > 1$  iteration, i.e.,  $\psi \leftarrow \alpha\psi + (1 - \alpha)\theta$ . Rather than hosting another VLM or pre-trained CLIP as a teacher model, we employ a self-evolving EMA network as a teacher, in accordance with the emerging evidence of the impressive robustness of weight-space ensembling among identical structure networks (Wortsman et al., 2022; Ramé et al., 2023). With the EMA teacher  $\psi$  and the learning student  $\theta$ , we construct a self-distillation loss term for a minibatch  $\mathcal{B}$  as:

$$\mathcal{L}_{SD}(\mathcal{B}, \theta) := \sum_{i=1}^B [KL(\tilde{q}_i^I || q_i^I) + KL(\tilde{q}_i^T || q_i^T)], \quad (2)$$

where  $KL$  denotes Kullback–Leibler divergence, student outputs are  $q_i^I = \text{softmax}(\{f_{\theta_v}(I_i) \cdot g_{\theta_t}(T_j)\}_{j=1}^B)$  and  $q_i^T = \text{softmax}(\{f_{\theta_v}(I_j) \cdot g_{\theta_t}(T_i)\}_{j=1}^B)$ , and teacher outputs  $\tilde{q}_j^I$  and  $\tilde{q}_j^T$  are similarly defined by replacing the student parameter  $\theta$  with teacher  $\psi$ . We complete the learning objective as a summation of  $\mathcal{L}_{CL}$  and  $\mathcal{L}_{SD}$  with a distillation coefficient  $\lambda$ , i.e.,  $\mathcal{L} = \mathcal{L}_{CL} + \lambda\mathcal{L}_{SD}$ . While this type of objective function is already adopted by Cheng et al. (2021) aiming at data-efficient supervision during pre-training, we design this method, **CaRot**, from a context of **calibrated robust fine-tuning** under distribution shift driven by our theoretical analysis on OOD calibration and classification error bound in § 3. In Figure 3, we provide empirical evidence to support the design motivation of our method by showing that CaRot achieves robust prediction against distribution shift (implying low  $\mathcal{H}$ -divergence) and low ID calibration error, thereby inducing good OOD calibration.

## 5. Experiments

### 5.1. Setup

**Training and evaluation.** We adopt CLIP ViT-B/16 as our VLM backbone and evaluate each fine-tuning method, including CaRot, in terms of calibration (with ECE) and accuracy under distribution shift. For downstream tasks, we

Table 3: Adversarial robustness after adversarial training. ID and OOD indicate IN and IN-Sketch, respectively. We generate adversarial examples of each ID data point with the 2-step projected gradient descent (PGD) algorithm with  $\text{stepsize}=1/255$  during training and evaluate the model under 10-step PGD adversarial examples of ID and OOD datasets.

Method	$L_\infty$ -norm bound = 1/255				$L_\infty$ -norm norm bound = 4/255			
	ID Acc.	OOD Acc.	ID ECE	OOD ECE	ID Acc.	OOD Acc.	ID ECE	OOD ECE
ZS	0.1583	0.2868	0.4252	0.2224	0.0124	0.1284	0.7641	0.4423
FT	0.6623	0.3539	0.1903	0.3133	0.4318	0.2850	0.4201	0.4432
LP-FT	0.6786	0.3967	0.1518	0.2764	0.4344	0.3019	0.3756	0.3964
FLYP	0.6774	0.4107	0.1219	0.2375	0.4477	0.3174	0.2980	0.3426
<b>CaRot</b>	<b>0.6870</b>	<b>0.4404</b>	<b>0.1028</b>	<b>0.1515</b>	<b>0.4522</b>	<b>0.3484</b>	<b>0.2182</b>	<b>0.2064</b>

consider the ImageNet-1K (IN) classification and regard it as our ID domain. For all methods, we optimize the model parameters using AdamW optimizer with a batch size of 512 over 10 epochs. The fine-tuned models are evaluated under three types of distribution shifts (OOD): natural shift, synthetic shift, and adversarial attack. For hyperparameter tuning, we use the validation split of IN.

**Dataset.** For natural shift, we consider IN-V2 (Recht et al., 2019), IN-R (Hendrycks et al., 2021a), IN-A (Hendrycks et al., 2021b), IN-Sketch (Wang et al., 2019), and ObjectNet (Barbu et al., 2019). For synthetic shift, we consider IN-C (Hendrycks & Dietterich, 2019) benchmark that contains 15 types of corruptions in five severity levels for each corruption. Following Hendrycks & Dietterich (2019), we report predictive performance using mean corruption error (mCE). We use four hold-out corruptions as our evaluation targets. For adversarial attack setting, following the setup of Mao et al. (2022), we generate  $L_\infty = 1/255$  bounded adversarial examples with 2-step PGD attack (Madry et al., 2017) with step size of  $1/255$  during train-time. We evaluate those adversarial training models with the same configuration of 10-step PGD attack-generated samples. For all datasets, except for IN-C, we report top-1 accuracy as a predictive performance metric and ECE as a metric for calibration.

**Baseline.** We benchmark CaRot alongside zero-shot inference (ZS) and fine-tuning methods: standard fine-tuning (FT), LP-FT (Kumar et al., 2022), and FLYP (Goyal et al., 2023). Furthermore, we compare each fine-tuning method with (*w/*) and without (*w/o*), applying post-hoc techniques for robustness (weight ensembling, WiSE-FT; Wortsman et al. (2022)) and post-hoc calibration (temperature scaling, TS; Guo et al. (2017)) method. Also, we compare our method with label smoothing (LS; Szegedy et al. (2016)) in the ablation study to validate the effectiveness of our input-dependent smoothing method. Refer § A for further details of each method.

## 5.2. Results on natural shift

**CaRot consistently outperforms robust fine-tuning methods for accuracy and ECE on both ID and OOD.** In Table 1, the comparison of accuracy and ECE results without TS and without ensemble highlights our argument. Existing robust fine-tuning methods make models miscalibrated, especially for OOD data, but CaRot successfully mitigates the miscalibration on ID dataset with the aid of self-distillation, and further transfers its calibration on OOD domains. Besides, CaRot shows a significant improvement in OOD accuracy, which is also expected from the results of theoretical analysis on classification error bound (§ 3).

**Effect of temperature scaling.** Comparing ECE values without and with TS from Table 1, applying TS generally improves both ID and OOD ECE except for CaRot, where TS shows more significant impact on other baselines than on CaRot. A possible explanation is that since confidence scores are already well-adjusted by learning from the input-dependent prior, further scaling the confidence score up/down for all data instances does not positively contribute to calibration as it does for other baselines. Notably, CaRot without TS outperforms all baselines (even with TS), in terms of OOD ECE. In Table 8, we also report OOD ECE where temperature values are tuned for each OOD dataset (i.e., empirical oracle setting that provides the upper bound of TS). Comparing the OOD ECE when tuned on ID and OOD, we see that selecting the proper temperature value for each domain is crucial for TS. Thus, under the environment where we can only access the ID domain, TS cannot guarantee good OOD calibration whereas CaRot can achieve robust calibration results under that environment.

**Effect of weight ensembling.** Comparing the results without (upper four rows) and with (bottom four rows) weight ensembling (WiSE-FT) of Table 1, we observe that WiSE-FT consistently improves OOD accuracy and ECE while somewhat tradeoffs ID accuracy and ECE. The impact of WiSE-FT is relatively small for CaRot. In fact, distilling the outputs of the EMA model to the student model could

Table 4: Ablation on EMA teacher update frequency (left) and self-distillation coefficient (right) under natural shift.  $\times$  denotes no EMA update for the teacher model and default values are colored in gray.

EMA freq.	Acc. ( $\uparrow$ )		ECE ( $\downarrow$ )		Distill coef.	Acc. ( $\uparrow$ )		ECE ( $\downarrow$ )	
	ID	OOD	ID	OOD		ID	OOD	ID	OOD
no distill	0.8258	0.5946	0.0643	0.1831	0.0	0.8258	0.5946	0.0643	0.1831
$\times$	0.7848	0.6199	0.1257	0.0936	0.5	0.8317	0.6134	0.0454	0.1365
1000	0.8286	<b>0.6302</b>	0.0696	<b>0.0790</b>	0.75	0.8319	0.6197	<b>0.0395</b>	0.1093
500	<b>0.8337</b>	0.6222	<b>0.0408</b>	0.0916	1.0	<b>0.8337</b>	0.6222	0.0408	0.0916
1	0.8250	0.5938	0.0649	0.1835	2.0	0.8277	<b>0.6247</b>	0.0747	<b>0.0796</b>

Table 5: Ablation study on each component of CaRot under natural shift.

	Method	Acc. ( $\uparrow$ )		ECE ( $\downarrow$ )	
		ID	OOD	ID	OOD
	ZS	0.6832	0.5840	0.0571	0.0836
CE	Hard label	0.8153	0.5750	0.0884	0.2186
	Label smoothing (LS)	0.8223	0.5833	0.0460	0.1147
	SWA	0.8173	0.5868	0.0836	0.2095
	EMA self-distil	0.8210	0.6054	0.0530	0.1560
CL	Hard label	0.8258	0.5946	0.0643	0.1831
	Label smoothing (LS)	0.8271	0.5975	0.0459	0.1295
	SWA	0.8248	0.5977	0.0634	0.1778
	EMA self-distil (Ours)	<b>0.8337</b>	<b>0.6222</b>	<b>0.0408</b>	<b>0.0916</b>

act as an implicit weight averaging by pushing the learning parameters toward the ensemble of the pre-trained and fine-tuning model. That is, the parameters of CaRot may already be closer to the pre-trained model than other fine-tuned methods, which is a source of additional robustness. Still, the CaRot can enjoy the benefits of weight ensemble in a situation where the OOD robustness is more crucial than ID adaptation.

### 5.3. Results on synthetic shift and adversarial attack

We provide results on synthetic shift (IN-C) and adversarial attack settings in Table 2 and Table 3, respectively. Similar to natural shift evaluation, CaRot consistently outperforms baselines in both scenarios. This result demonstrates that CaRot is a general method that covers diverse types of distribution shifts. Moreover, CaRot’s notable performance under adversarial attacks aligns with recent findings (Wang et al., 2024) that the generalizable features of a pre-trained model can contribute to the adversarial robustness of the fine-tuning model. Additional results on IN-C for different severity levels of corruption are depicted in Figure 5.

### 5.4. Ablation study

Table 5 shows an ablation study on each component of CaRot. We see that adopting contrastive learning with EMA

self-distillation shows the best result compared with varying learning objectives (cross-entropy (CE) vs. contrastive learning (CL)) and types of label (hard label vs. standard LS vs. EMA self-distillation). CE-based learning refers to the standard fine-tuning (see § A for details). For distillation over CE, we use only an image encoder as a teacher model. Accordingly, only image-to-text distillation is applied, and only the image encoder is updated through EMA.

Our observation that adopting contrastive learning for fine-tuning improves accuracy both on ID and OOD datasets is consistent with previous work (Goyal et al., 2023). Furthermore, we discover that calibration on the ID setting is much better when using CL than CE. Moreover, we see that using soft labels obtained from the EMA updated teacher model is more favorable compared with both hard and uniformly soft labels of LS. More results with different LS parameters is provided in Table 6.

To investigate the effect of self-distillation, we report the performance of weight averaged model without train-time regularization, i.e., no distillation that we denote as SWA (Izmailov et al., 2018) in Table 5. Here, the evaluation is done with EMA updated teacher model directly. From the empirical result, we conclude that distillation from teacher model output is a key factor of improved performance, not just gradually averaging the fine-tuned model with the previous model.

Table 4 shows the sensitivity of our model regarding the important hyperparameters: EMA update frequency and the strength of self-distillation loss. Since two hyperparameters affect each other, we first search for a more sensitive parameter — EMA update frequency and then set the distillation coefficient. Distillation with the fixed pre-trained model (left side of Table 4 denoted with  $\times$ ) does not help the model to adapt to ID downstream task. On the other hand, updating the teacher model too frequently deteriorates OOD performance (both accuracy and ECE). Distillation strength shows a more significant impact on ECE, which supports our rationale to adopt self-distillation to improve confidence calibration. We set this value as 1.0 to match scales of contrastive and distillation losses.



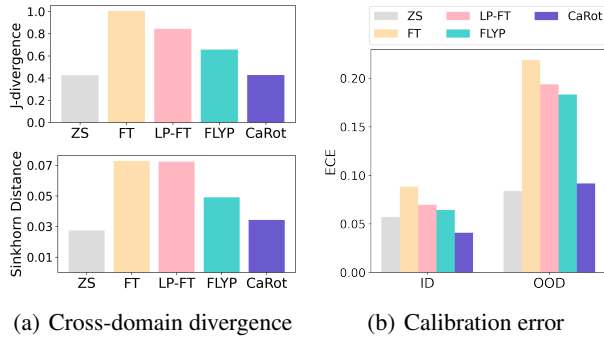


Figure 3: (a) For each model, we measured a J-divergence (symmetrized version of KL divergence) and Sinkhorn distance between output probability from two different domains: IN and IN-C. (b) We visualize ECE of each method on ID (IN) and OOD (natural shift) datasets (the actual values are the same as those in Table 1 w/o TS.)

### 5.5. Supporting evidence for theoretical analysis

In § 3, we identify the OOD calibration error (and the sum of OOD classification error and prediction sharpness) can be bounded above the summation of (i) ID calibration error, (ii) divergence, and other irreducible terms. In Figure 3, we show that by leveraging self-distillation as an input-dependent regularization, CaRot achieves a low ID calibration error compared to other methods (in all the previous tables and Figure 3 (b)). Moreover, CaRot induces a robust prediction across ID and OOD domains, i.e., CaRot shows relatively small pair-wise J-divergence and Sinkhorn distance, the proxy of  $\mathcal{H}$ -divergence, on the softmax output between the validation samples from ImageNet and ImageNet-C (Figure 3 (a)). By effectively reducing two terms (i) and (ii), CaRot reduces the upper bound of OOD calibration and classification (with prediction sharpness) errors. Therefore, our theoretical analysis, supported by abundant empirical evidence, justifies the use of CaRot for calibrated robust fine-tuning of visual foundation models under distribution shifts.

### 5.6. Additional results

We summarize additional experiment results in Figure 4 highlighting the calibration error. More results including the accuracy are provided in Appendix Figure 5, 6, 7, and 8 for each of Figure 4 (a-d), respectively.

Figure 4 (a) shows the impact of the label smoothing parameter under natural shift. CaRot consistently shows lower calibration error on both ID and OOD. This result emphasizes that input-dependent label smoothing improves calibration better than uniform label smoothing. We investigate the impact of the batch size under natural shift (Figure 4 (b)). The larger the batch size is, CaRot shows the more robust calibra-

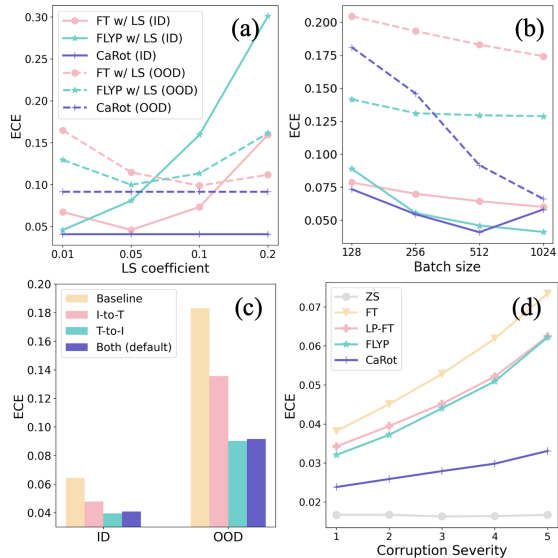


Figure 4: ECE with various LS coef. (a), training batch size (b), and distillation term (c) under natural shift. IN-C ECE for different severities (d). (a) and (b) share the legend.

tion for ID and OOD. This supports our rationale for employing input-dependent label smoothing with contrastive loss to promote learning a data structure by contrasting diverse in-batch relations. Self-distillation loss (Eq. 2) consists of two terms: image-to-text and text-to-image. We analyzed the impact of each term. As depicted in Figure 4 (c), distilling text-to-image probability (produced by contrasting one text to multiple in-batch images) showed a more significant effect on improving calibration than distilling image-to-text probability (produced by contrasting one image to multiple in-batch text). In terms of accuracy, adopting both directions of distribution achieves the best result (see Figure 7). Finally, detailed ImageNet-C results for different severities are provided in Figure 4 (d). CaRot consistently shows low and robust calibration errors across all severity levels.

## 6. Discussion

The unreliable predictive uncertainty (confidence) of deep learning models is one of the key obstacles to pursuing trustworthy artificial intelligence in real-world. We raise concern for miscalibration issues, especially under distribution shifts, of robust fine-tuning methods for visual foundation models. Furthermore, we specify the key factors of calibration on unseen domains. From this analysis, we devise a calibrated robust fine-tuning method, called **CaRot**, that improves not only the accuracy but also calibration on both ID and OOD domains through learning objectives that pursue OOD robustness and ID calibration. Across comprehensive experiments, CaRot shows superior results and we theoretically explain CaRot’s remarkable empirical success.



**Limitations and future work.** While there are numerous VLMs beyond CLIP (Radford et al., 2021), we confine the scope of validation to image classification with CLIP ViT-B/16 following conventional evaluation setup of previous works on robust fine-tuning (Kumar et al., 2022; Wortsman et al., 2022; Goyal et al., 2023). We leave the investigation on whether CaRot can still be effective for confidence calibration of other VLMs or not as a future work.

## Impact Statements

For reliable machine learning in the wild, robustness under distribution shifts is crucial. Moreover, ensuring the calibration of model prediction is an inevitable step for broadening the application of artificial intelligence toward real-world decision-making systems. In this work, we provide an effective approach to pursuing robustness and calibration in a unified framework for fine-tuning VLMs. We expect that the proposed method can positively affect the push of a boundary for ML applications. However, the inherent biases from the pre-trained model could still have the potential risk of negatively affecting downstream social applications even after fine-tuning with our method.

## References

- Barbu, A., Mayo, D., Alverio, J., Luo, W., Wang, C., Gutfreund, D., Tenenbaum, J., and Katz, B. Objectnet: A large-scale bias-controlled dataset for pushing the limits of object recognition models. In *Advances in Neural Information Processing Systems (NeurIPS)*, 2019.
- Ben-David, S., Blitzer, J., Crammer, K., Kulesza, A., Pereira, F., and Vaughan, J. A theory of learning from different domains. *Machine Learning*, 79:151–175, 05 2010. doi: 10.1007/s10994-009-5152-4.
- Bommasani, R., Hudson, D. A., Adeli, E., Altman, R., Arora, S., von Arx, S., Bernstein, M. S., Bohg, J., Bosselut, A., Brunskill, E., et al. On the opportunities and risks of foundation models. *arXiv preprint arXiv:2108.07258*, 2021.
- Cheng, R., Wu, B., Zhang, P., Vajda, P., and Gonzalez, J. E. Data-efficient language-supervised zero-shot learning with self-distillation. In *Proceedings of the IEEE/CVF Conference on Computer Vision and Pattern Recognition (CVPR) Workshops*, 2021.
- DeGroot, M. H. and Fienberg, S. E. The comparison and evaluation of forecasters. *Journal of the Royal Statistical Society. Series D (The Statistician)*, 1983. ISSN 00390526, 14679884.
- Deng, J., Dong, W., Socher, R., Li, L.-J., Li, K., and Fei-Fei, L. Imagenet: A large-scale hierarchical image database. In *IEEE Conference on Computer Vision and Pattern Recognition (CVPR)*, 2009.
- Gong, Y., Lin, X., Yao, Y., Dietterich, T. G., Divakaran, A., and Gervasio, M. Confidence calibration for domain generalization under covariate shift. In *IEEE Conference on Computer Vision and Pattern Recognition (CVPR)*, 2021.
- Goyal, S., Kumar, A., Garg, S., Kolter, Z., and Raghunathan, A. Finetune like you pretrain: Improved finetuning of zero-shot vision models. In *IEEE Conference on Computer Vision and Pattern Recognition (CVPR)*, 2023.
- Guo, C., Pleiss, G., Sun, Y., and Weinberger, K. Q. On calibration of modern neural networks. In *International Conference on Machine Learning (ICML)*, 2017.
- Guo, H., Pasunuru, R., and Bansal, M. An overview of uncertainty calibration for text classification and the role of distillation. In *Proceedings of the 6th Workshop on Representation Learning for NLP (ReplANLP-2021)*, 2021.
- Gupta, K., Rahimi, A., Ajanthan, T., Mensink, T., Sminchisescu, C., and Hartley, R. Calibration of neural networks using splines. *arXiv preprint arXiv:2006.12800*, 2020.
- Hendrycks, D. and Dietterich, T. Benchmarking neural network robustness to common corruptions and perturbations. *arXiv preprint arXiv:1903.12261*, 2019.
- Hendrycks, D., Basart, S., Mu, N., Kadavath, S., Wang, F., Dorundo, E., Desai, R., Zhu, T., Parajuli, S., Guo, M., et al. The many faces of robustness: A critical analysis of out-of-distribution generalization. In *IEEE Conference on Computer Vision and Pattern Recognition (CVPR)*, 2021a.
- Hendrycks, D., Zhao, K., Basart, S., Steinhardt, J., and Song, D. Natural adversarial examples. In *IEEE Conference on Computer Vision and Pattern Recognition (CVPR)*, 2021b.
- Izmailov, P., Wilson, A., Podoprikin, D., Vetrov, D., and Gariipov, T. Averaging weights leads to wider optima and better generalization. In *Uncertainty in Artificial Intelligence (UAI)*, 2018.
- Joy, T., Pinto, F., Lim, S.-N., Torr, P. H., and Dokania, P. K. Sample-dependent adaptive temperature scaling for improved calibration. In *AAAI Conference on Artificial Intelligence (AAAI)*, 2023.
- Kingma, D. P. and Welling, M. Auto-encoding variational bayes. *arXiv preprint arXiv:1312.6114*, 2013.
- Kull, M., Perello Nieto, M., Kängsepp, M., Silva Filho, T., Song, H., and Flach, P. Beyond temperature scaling:

- Obtaining well-calibrated multi-class probabilities with dirichlet calibration. *Advances in Neural Information Processing Systems (NeurIPS)*, 2019.
- Kumar, A., Raghunathan, A., Jones, R., Ma, T., and Liang, P. Fine-tuning can distort pretrained features and underperform out-of-distribution. In *International Conference on Learning Representations (ICLR)*, 2022.
- Lee, Y., Chen, A. S., Tajwar, F., Kumar, A., Yao, H., Liang, P., and Finn, C. Surgical fine-tuning improves adaptation to distribution shifts. In *International Conference on Learning Representations (ICLR)*, 2023.
- LeVine, W., Pikus, B., Raj, P., and Gil, F. A. Enabling calibration in the zero-shot inference of large vision-language models. *arXiv preprint arXiv:2303.12748*, 2023.
- Madry, A., Makelov, A., Schmidt, L., Tsipras, D., and Vladu, A. Towards deep learning models resistant to adversarial attacks. *arXiv preprint arXiv:1706.06083*, 2017.
- Mao, C., Geng, S., Yang, J., Wang, X., and Vondrick, C. Understanding zero-shot adversarial robustness for large-scale models. In *International Conference on Learning Representations (ICLR)*, 2022.
- Minderer, M., Djolonga, J., Romijnders, R., Hubis, F., Zhai, X., Houlsby, N., Tran, D., and Lucic, M. Revisiting the calibration of modern neural networks. *Advances in Neural Information Processing Systems (NeurIPS)*, 34, 2021.
- Mohri, M., Rostamizadeh, A., and Talwalkar, A. *Foundations of machine learning*. MIT press, 2018.
- Mukhoti, J., Kulharia, V., Sanyal, A., Golodetz, S., Torr, P., and Dokania, P. Calibrating deep neural networks using focal loss. *Advances in Neural Information Processing Systems (NeurIPS)*, 2020.
- Müller, R., Kornblith, S., and Hinton, G. E. When does label smoothing help? *Advances in Neural Information Processing Systems (NeurIPS)*, 2019.
- Murphy, A. H. Scalar and vector partitions of the probability score : Part i. two-state situation. *Journal of Applied Meteorology (1962-1982)*, 1972.
- Naeini, M. P., Cooper, G., and Hauskrecht, M. Obtaining well calibrated probabilities using bayesian binning. In *AAAI Conference on Artificial Intelligence (AAAI)*, 2015.
- Niculescu-Mizil, A. and Caruana, R. Predicting good probabilities with supervised learning. In *International Conference on Machine Learning (ICML)*, 2005.
- Oh, C., So, J., Lim, Y., Byun, H., Shin, M., Jeon, J.-J., and Song, K. Geodesic multi-modal mixup for robust fine-tuning. *Advances in Neural Information Processing Systems (NeurIPS)*, 2023.
- Park, S., Bastani, O., Weimer, J., and Lee, I. Calibrated prediction with covariate shift via unsupervised domain adaptation. In *International Conference on Artificial Intelligence and Statistics (AISTATS)*, 2020.
- Radford, A., Kim, J. W., Hallacy, C., Ramesh, A., Goh, G., Agarwal, S., Sastry, G., Askell, A., Mishkin, P., Clark, J., et al. Learning transferable visual models from natural language supervision. In *International Conference on Machine Learning (ICML)*, 2021.
- Ram'e, A., Ahuja, K., Zhang, J., Cord, M., Bottou, L., and Lopez-Paz, D. Model ratatouille: Recycling diverse models for out-of-distribution generalization. In *International Conference on Machine Learning (ICML)*, 2023.
- Recht, B., Roelofs, R., Schmidt, L., and Shankar, V. Do imagenet classifiers generalize to imagenet? In *International Conference on Machine Learning (ICML)*, 2019.
- Sanders, F. On subjective probability forecasting. *Journal of Applied Meteorology (1962-1982)*, (2):191–201, 1963.
- Sensoy, M., Kaplan, L., and Kandemir, M. Evidential deep learning to quantify classification uncertainty. *Advances in Neural Information Processing Systems (NeurIPS)*, 2018.
- Szegedy, C., Vanhoucke, V., Ioffe, S., Shlens, J., and Wojna, Z. Rethinking the inception architecture for computer vision. In *IEEE Conference on Computer Vision and Pattern Recognition (CVPR)*, 2016.
- Thulasidasan, S., Chennupati, G., Bilmes, J. A., Bhattacharya, T., and Michalak, S. On mixup training: Improved calibration and predictive uncertainty for deep neural networks. *Advances in Neural Information Processing Systems (NeurIPS)*, 2019.
- Tian, J., He, Z., Dai, X., Ma, C.-Y., Liu, Y.-C., and Kira, Z. Trainable projected gradient method for robust fine-tuning. In *IEEE Conference on Computer Vision and Pattern Recognition (CVPR)*, 2023a.
- Tian, J., Liu, Y.-C., Smith, J., and Kira, Z. Fast trainable projection for robust fine-tuning. In *Advances in Neural Information Processing Systems (NeurIPS)*, 2023b.
- Tomani, C., Gruber, S., Erdem, M. E., Cremers, D., and Buettner, F. Post-hoc uncertainty calibration for domain drift scenarios. In *IEEE Conference on Computer Vision and Pattern Recognition (CVPR)*, 2021.

- Wang, H., Ge, S., Lipton, Z., and Xing, E. P. Learning robust global representations by penalizing local predictive power. In *Advances in Neural Information Processing Systems (NeurIPS)*, 2019.
- Wang, S., Zhang, J., Yuan, Z., and Shan, S. Pre-trained model guided fine-tuning for zero-shot adversarial robustness. *arXiv preprint arXiv:2401.04350*, 2024.
- Wortsman, M., Ilharco, G., Kim, J. W., Li, M., Kornblith, S., Roelofs, R., Lopes, R. G., Hajishirzi, H., Farhadi, A., Namkoong, H., et al. Robust fine-tuning of zero-shot models. In *IEEE Conference on Computer Vision and Pattern Recognition (CVPR)*, 2022.
- Yu, Y., Bates, S., Ma, Y., and Jordan, M. Robust calibration with multi-domain temperature scaling. *Advances in Neural Information Processing Systems (NeurIPS)*, 2022.
- Yuan, L., Tay, F. E., Li, G., Wang, T., and Feng, J. Revisiting knowledge distillation via label smoothing regularization. In *IEEE Conference on Computer Vision and Pattern Recognition (CVPR)*, 2020.
- Zadrozny, B. and Elkan, C. Transforming classifier scores into accurate multiclass probability estimates. In *ACM SIGKDD International Conference on Knowledge Discovery and Data Mining (KDD)*, 2002.
- Zhang, C.-B., Jiang, P.-T., Hou, Q., Wei, Y., Han, Q., Li, Z., and Cheng, M.-M. Delving deep into label smoothing. *IEEE Transactions on Image Processing*, 2021.
- Zhang, H., Cisse, M., Dauphin, Y. N., and Lopez-Paz, D. mixup: Beyond empirical risk minimization. *arXiv preprint arXiv:1710.09412*, 2017.
- Zhang, J., Kailkhura, B., and Han, T. Y.-J. Mix-n-match: Ensemble and compositional methods for uncertainty calibration in deep learning. In *International Conference on Machine Learning (ICML)*, 2020.
- Zhang, Z. and Sabuncu, M. Self-distillation as instance-specific label smoothing. In *Advances in Neural Information Processing Systems (NeurIPS)*, 2020.
- Zhao, H., Zhang, S., Wu, G., Moura, J. M. F., Costeira, J. P., and Gordon, G. J. Adversarial multiple source domain adaptation. In *Advances in Neural Information Processing Systems (NeurIPS)*, 2018.

## A. Experimental Detail

### A.1. Evaluation data

Training and test splits of ImageNet-1K (Deng et al., 2009) consist of 1000 classes and its variants have the entire 1000 or a subset of the classes. Following Radford et al. (2021) and Goyal et al. (2023), we use OpenAI template to create text descriptions for each class (80 templates per class) for evaluation and the averaged text representation is used as a final class representation for evaluation.

### A.2. Baseline methods

**Zero-shot (ZS; Radford et al. (2021)):** Zero-shot classifier is obtained by encoding and averaging text representations of each class using pre-trained CLIP text encoder.

**Standard fine-tuning (FT; Wortsman et al. (2022)):** Linear classification head is initialized with text representation vectors for each class encoded by pre-trained CLIP text encoder. Image encoder and linear classifier parameters are fine-tuned for 10 epochs with a learning rate  $3e-5$ .

**LP-FT (Kumar et al., 2022):** Randomly initialized linear classification head is first trained upon frozen image encoder for 5 epochs and then both image encoder and linear head parameters are updated for 5 epochs. For each phase, we use a learning rate of  $1e-2$  and  $3e-5$ , respectively.

**Fine-tuning with contrastive learning (FLYP; Goyal et al. (2023)):** Both image and text encoders are updated without additional linear classification head. To create text representation of training samples, we use OpenAI template similar to the evaluation data. Unlike for evaluation, we do not take the average of 80 different templates. Training pairs are randomly selected throughout the training steps. We fine-tune the model for 10 epochs (in total, 25K steps) with a learning rate of  $1e-5$ .

**CaRot (Ours):** We set the distill coefficient ( $\lambda$ ) as 1.0, EMA update frequency as 500, and EMA final target momentum as 0.9. We linearly increased the EMA momentum  $\alpha$  by 0.05 for the first 20% iterations. We followed all the other details from FLYP.

Furthermore, we compare the fine-tuning methods with and without applying post-hoc techniques for robustness (weight ensembling) and calibration (temperature scaling). Moreover, in ablation, we compare our self-distillation based soft label with uniform constant label smoothing.

**Weight average of fine-tuned and zero-shot (ensemble; (Wortsman et al., 2022)):** Zero-shot and fine-tuned model weights are averaged with strength of  $\alpha_{\text{ensemble}}$ . Since this ensembling technique can be applied to any fine-tuning method.  $\alpha_{\text{ensemble}}$  is set as 0.5 for all methods. More results with different  $\alpha_{\text{ensemble}}$  is provided in Table 9.

**Temperature scaling (TS; Guo et al. (2017)):** Before applying the softmax function to compute output probability distribution, TS divides the logit by temperature  $\tau \in (0, \infty)$ .  $\tau \rightarrow 0$  makes the probability similar to point masses (sharpening),  $\tau \rightarrow \infty$  makes uniform distribution (smoothing). Scaling the output distribution does not affect accuracy since it does not change the model prediction (i.e., the probability rank remains the same). Temperature value was tuned for each method on ID validation set w.r.t. negative log-likelihood (NLL).

**Label smoothing (LS; Szegedy et al. (2016)):** LS is a regularization strategy that pursues the generalization of classification by utilizing *soft label*, which is derived by adding uniform distribution to the hard label distribution. The soft label can be viewed as a new target probability distribution where the value of 1 to the target pair is reduced and the value of 0 for the non-target pair is increased by the smoothing parameter  $\epsilon \in (0, 1)$ . Since utilizing soft labels allows the model to pull negative pairs with limited strength, LS is beneficial for calibration beyond generalization by addressing over-confidence issue (Müller et al., 2019).

## B. Detailed Analysis for Each OOD Data

### B.1. Accuracy and ECE for each OOD Data

Our method demonstrated superior performance in terms of averaged accuracy and ECE for both ID and OOD data as shown in Table 1. In this section, we present more specific results, detailing the accuracy and ECE results across various types of OOD data. The accuracy results are presented in Table 6, while the ECE results are shown in Table 7 (without TS) and



Table 8 (with TS). We report ECE with TS results in two cases: temperature scaled with ID ECE and scaled with OOD NLL (oracle setting).

Table 6: Detailed OOD accuracy for natural shift

Acc. ( $\uparrow$ )							
Method	ID		OOD				
	avg	avg	ImageNetV2	ImageNetR	ImageNetA	ImageNetSketch	ObjectNet
ZS	0.6832	0.5840	0.6193	0.7771	0.4995	0.4826	0.5417
<i>w/o ensemble</i>							
FT	0.8153	0.5750	0.7166	0.7014	0.4401	0.4911	0.5256
LP-FT	0.8217	0.5822	0.7206	0.7047	0.4629	0.4868	0.5360
FLYP	0.8258	0.5946	0.7273	0.7135	0.4852	0.4984	0.5486
<b>CaRot</b>	<b>0.8337</b>	<b>0.6222</b>	<b>0.7446</b>	<b>0.7646</b>	<b>0.5137</b>	<b>0.5235</b>	<b>0.5650</b>
<i>w/ ensemble (WiSE-FT <math>\alpha_{ensemble} = 0.5</math>)</i>							
FT	0.8043	0.6350	0.7194	0.7926	0.5449	0.5369	0.5814
LP-FT	<b>0.8197</b>	0.6003	0.7182	0.7291	0.5044	0.4975	0.5524
FLYP	0.8102	0.6423	0.7254	0.7970	0.5604	0.5384	<b>0.5901</b>
<b>CaRot</b>	0.8040	<b>0.6443</b>	<b>0.7261</b>	<b>0.8049</b>	<b>0.5616</b>	<b>0.5394</b>	0.5898

Table 7: Detailed OOD ECE for natural shift without temperature scaling

ECE ( $\downarrow$ ) <i>w/o TS</i>							
Method	ID		OOD				
	avg	avg	ImageNetV2	ImageNetR	ImageNetA	ImageNetSketch	ObjectNet
ZS	0.0571	0.0737	0.0548	0.0541	0.0967	0.0850	0.0780
<i>w/o ensemble</i>							
FT	0.0884	0.2186	0.1468	0.1164	0.3000	0.2544	0.2753
LP-FT	0.0696	0.1936	0.1222	0.1064	0.2697	0.2251	0.2447
FLYP	0.0643	0.1831	0.1171	0.0967	0.2435	0.2200	0.2383
<b>CaRot</b>	<b>0.0408</b>	<b>0.0916</b>	<b>0.0492</b>	<b>0.0412</b>	<b>0.1492</b>	<b>0.0833</b>	<b>0.1355</b>
<i>w/ ensemble (WiSE-FT <math>\alpha_{ensemble} = 0.5</math>)</i>							
FT	0.2129	0.1764	0.1949	0.2040	0.1537	0.1918	0.1376
LP-FT	0.1921	0.1651	0.1767	0.2059	0.1385	0.1793	0.1252
FLYP	0.0794	0.1327	0.1006	0.0696	0.1681	0.1565	0.1687
<b>CaRot</b>	<b>0.0453</b>	<b>0.0759</b>	<b>0.0481</b>	<b>0.0424</b>	<b>0.1066</b>	<b>0.0806</b>	<b>0.1020</b>

Table 8: Detailed OOD ECE for natural shift with temperature scaling

ECE ( $\downarrow$ ) <i>w/ TS</i>													
Method	ID		temperature tuned with ID					temperature tuned with OOD					
	avg	avg	IN-V2	IN-R	IN-A	IN-Sketch	ObjectNet	oracle avg	IN-V2	IN-R	IN-A	IN-Sketch	ObjectNet
ZS	0.0392	0.1217	0.0633	0.0532	0.1792	0.1370	0.1760	0.0755	0.0459	0.1273	0.0894	0.0750	0.07554
<i>w/o ensemble</i>													
FT	0.0463	0.1259	0.0786	0.0484	0.1798	0.1408	0.1820	0.0701	0.0786	0.0484	0.0784	0.0724	0.0726
LP-FT	0.0382	0.0979	0.0509	0.0477	0.1450	0.1028	0.1433	0.0687	0.0509	0.0477	0.0798	0.1028	0.0624
FLYP	0.0392	0.1217	0.0633	0.0532	0.1792	0.1370	0.1760	0.0755	0.0401	0.0459	0.1273	0.0894	0.0750
<b>CaRot</b>	0.0397	0.0941	0.0513	0.0417	0.1532	0.0857	0.1386	0.0596	0.0402	0.0417	0.0796	0.0702	0.0661
<i>w/ ensemble (WiSE-FT <math>\alpha_{ensemble} = 0.5</math>)</i>													
FT	0.0423	0.0904	0.0600	0.0381	0.1256	0.1037	0.1246	0.0675	0.0462	0.0381	0.0864	0.0749	0.0917
LP-FT	0.0754	0.1276	0.0982	0.0501	0.1692	0.1565	0.1641	0.1209	0.0982	0.0501	0.1519	0.1774	0.1269
FLYP	0.0441	0.0856	0.0523	0.0381	0.1187	0.0967	0.1224	0.0563	0.0404	0.0381	0.0671	0.0748	0.0609
<b>CaRot</b>	0.0453	0.0774	0.0496	0.0407	0.1101	0.0819	0.1049	0.0669	0.0432	0.0375	0.1207	0.0761	0.0569

## B.2. Test Error and ECE by Corruption Severity

The ImageNet-C dataset features corruption severity levels ranging from 1 to 5. In Figure 5, we show the test error and ECE for each severity level, dividing the results into those with and without the application of ensemble. Compared to other methods, our approach exhibits the lowest test error across all severity levels. Furthermore, while other methods show a rapid increase in ECE as severity levels rise, our method demonstrates a relatively slower increase in ECE while conserving the lowest ECE, indicating its robustness against increasing corruption severity.

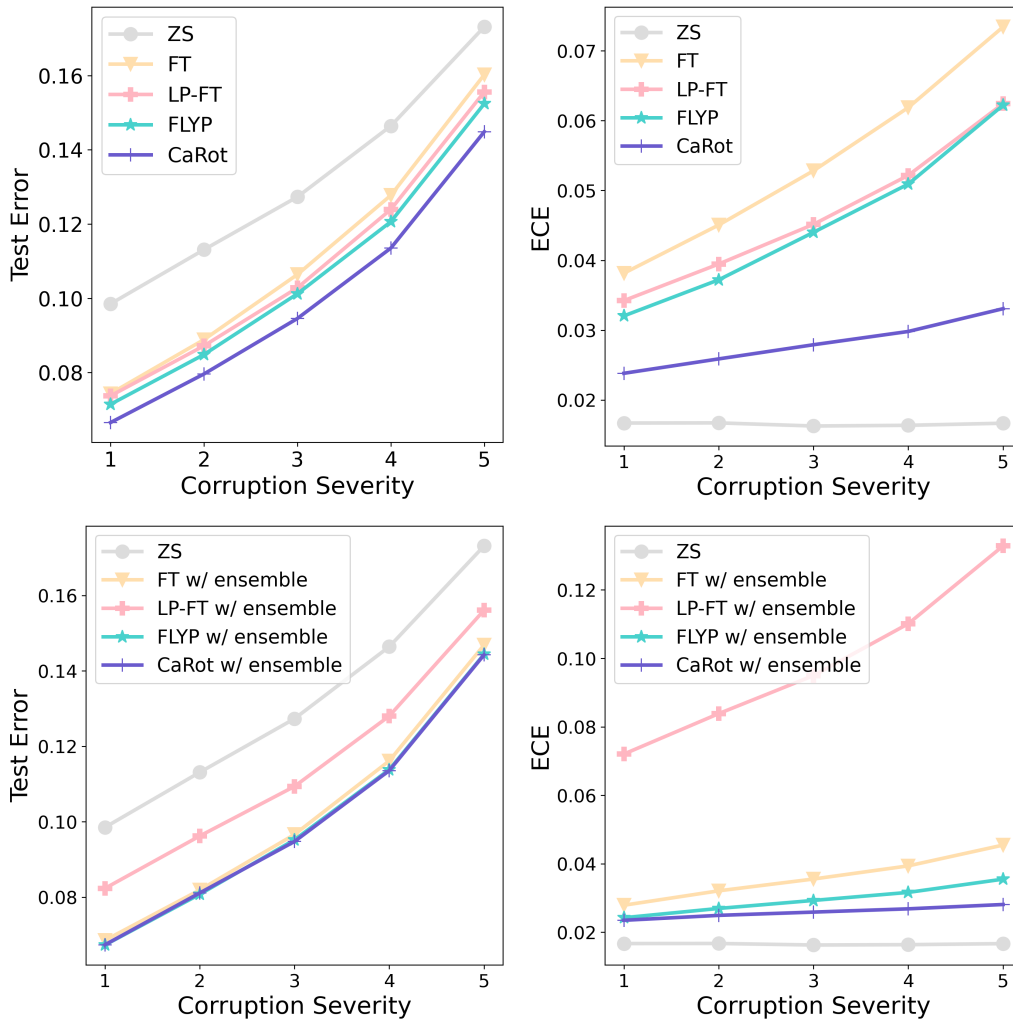


Figure 5: Test error and expected calibration error (ECE) of ImageNet fine-tuned CLIP ViT-B/16 on ImageNet-C.

## C. Ablation study on Hyperparameters

In this section, we present the results of thorough ablation studies on various hyperparameters associated with the methodologies addressed in our paper.

### C.1. Ablation study on Ensemble Strength $\alpha_{\text{ensemble}}$

We present the results based on the hyperparameter  $\alpha_{\text{ensemble}}$  when using the weight average of fine-tuned and zero-shot method (ensemble; (Wortsman et al., 2022)). As the  $\alpha_{\text{ensemble}}$  value increases, the ensemble weight on the fine-tuning model becomes larger. Since this method can be applied to any fine-tuning approaches, we conducted experiments with various  $\alpha_{\text{ensemble}}$  values ranging from 0.1 to 0.9 across all fine-tuning methods.

Table 9: Ablation study on Different ensemble strength  $\alpha_{\text{ensemble}}$ .

Method	$\alpha_{\text{ensemble}}$	ID Acc. ( $\uparrow$ )	ID ECE ( $\downarrow$ )	OOD Acc. ( $\uparrow$ )	OOD ECE ( $\downarrow$ )
FT	0.1	0.7157	0.7115	0.6019	0.5901
	0.2	0.7487	0.7268	0.6186	0.5800
	0.3	0.7716	0.6603	0.6290	0.5036
	0.4	0.7904	0.4440	0.6332	0.3371
	0.5	0.8043	0.2129	0.6350	0.1764
	0.6	0.8144	0.0979	0.6314	0.1111
	0.7	0.8196	0.0714	0.6236	0.1209
	0.8	0.8214	0.0772	0.6122	0.1552
	0.9	0.8206	0.0881	0.5958	0.1922
FLYP	0.1	0.7211	0.0961	0.6063	0.1132
	0.2	0.7514	0.0895	0.6225	0.1152
	0.3	0.7757	0.0849	0.6333	0.1181
	0.4	0.7955	0.0803	0.6405	0.1249
	0.5	0.8102	0.0794	0.6423	0.1327
	0.6	0.8196	0.0792	0.6407	0.1427
	0.7	0.8253	0.0773	0.6342	0.1530
	0.8	0.8291	0.0787	0.6252	0.1644
	0.9	0.8298	0.0798	0.6127	0.1788
LP-FT	0.1	0.6402	0.6336	0.4432	0.4280
	0.2	0.7759	0.7358	0.5589	0.5071
	0.3	0.8044	0.6185	0.5861	0.4313
	0.4	0.8147	0.3771	0.5960	0.2854
	0.5	0.8197	0.1921	0.6003	0.1651
	0.6	0.8225	0.1036	0.6016	0.1178
	0.7	0.8241	0.0727	0.6005	0.1182
	0.8	0.8239	0.0683	0.5976	0.1429
	0.9	0.8234	0.0759	0.5910	0.1735
CaRot	0.1	0.7184	0.054	0.6039	0.0733
	0.2	0.7468	0.0522	0.6195	0.0723
	0.3	0.7705	0.0492	0.6308	0.0727
	0.4	0.7894	0.0471	0.6394	0.0740
	0.5	0.8040	0.0453	0.6444	0.0759
	0.6	0.8157	0.0434	0.6451	0.0777
	0.7	0.8240	0.0412	0.6436	0.0805
	0.8	0.8292	0.0384	0.6383	0.0854
	0.9	0.8323	0.0399	0.6316	0.0890

### C.2. Ablation study on Label Smoothing Coefficient

We present the results based on the coefficient hyperparameter when using label smoothing (LS; Szegedy et al. (2016)). We conducted experiments with various LS coefficient values ranging from 0.01 to 0.2 across various fine-tuning method on both ID and OOD data. Figure 6 illustrates the accuracy and ECE by the label smoothing coefficient.

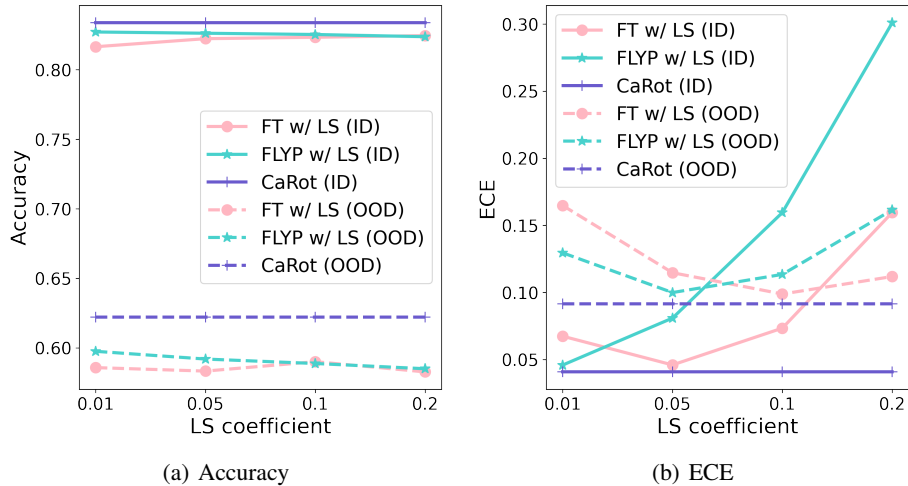


Figure 6: Ablation study on the label smoothing (LS; Szegedy et al. (2016)) coefficient.

### C.3. Ablation study on Knowledge Distillation strategy

CaRot conducts distillation of both the image-to-text and text-to-image logits, simultaneously. In this section, we ablate the analysis into image-to-text only and text-to-image only distillation, and compare these results with the result where both distillations were applied, illustrating differences in accuracy and ECE.

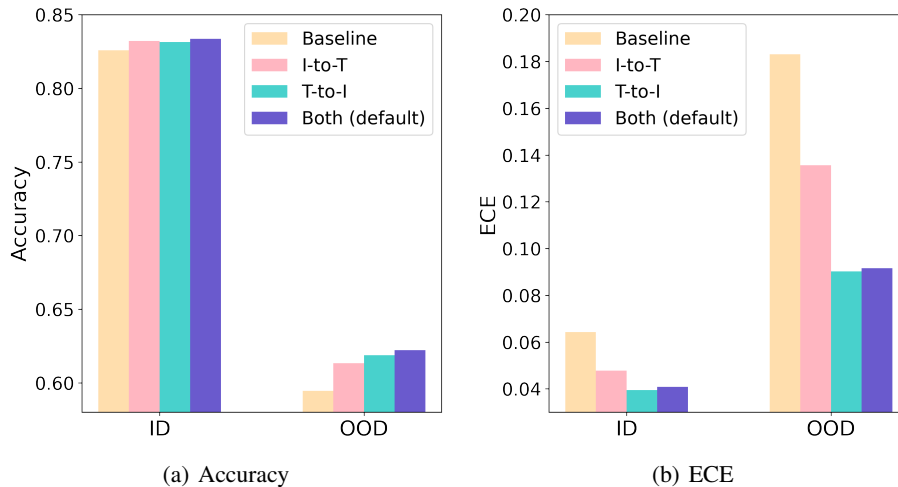


Figure 7: Ablation study on knowledge distillation strategy.

### C.4. Ablation study on Batch Size

We present the results based on various batch size when using fine-tuning method. We conducted experiments with batch sizes from 128 to 1024 on both ID and OOD data. The accuracy and ECE by the batch size are illustrated in Figure 8.



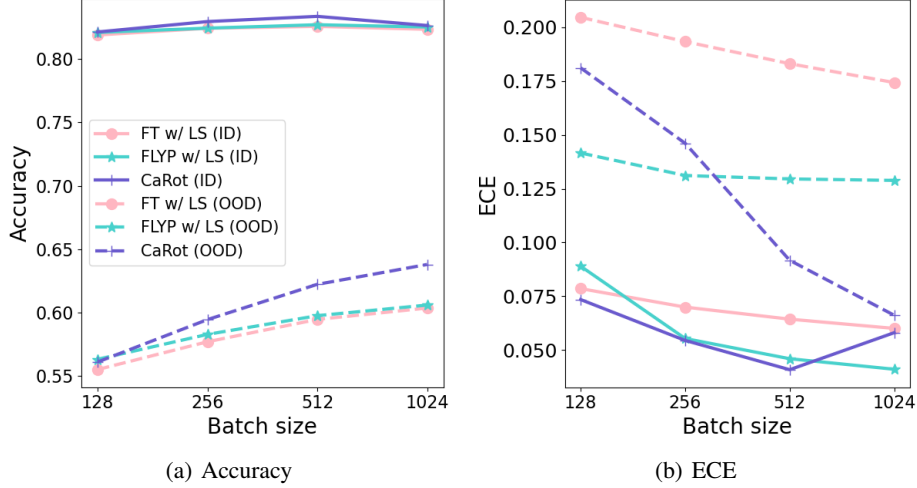


Figure 8: Ablation study on the batch size. (a) and (b) share the legend.

## D. Proof

In this section, we provide a proof for Theorem 3.

**Theorem D.1** (Restatement of Theorem 3.). *Let  $h : \mathcal{X} \rightarrow [0, 1]$  be a real-valued function in a hypothesis class  $\mathcal{H}$  with a pseudo dimension  $\mathcal{Pdim}(\mathcal{H}) = d$ . If  $\hat{\mathcal{D}}_{ID}$  and  $\hat{\mathcal{D}}_{OOD}$  are the empirical distributions constructed by  $n$ -size i.i.d. samples, drawn from  $\mathcal{D}_{ID}$  and  $\mathcal{D}_{OOD}$  respectively, then for any  $\delta \in (0, 1)$ , and for all  $h$ , two bounds below hold with probability at least  $1 - \delta$ .*

$$i) \varepsilon_{\mathcal{D}_{OOD}}(h) \leq \varepsilon_{\hat{\mathcal{D}}_{ID}}(h) + \frac{1}{2}d_{\bar{\mathcal{H}}}(\hat{\mathcal{D}}_{ID}, \hat{\mathcal{D}}_{OOD}) + \Delta + \mathcal{O}\left(\sqrt{\frac{d \log(n/d) + \log(1/\delta)}{n}}\right)$$

$$ii) \mathbb{E}_{\mathcal{D}_{OOD}}[|h(x) - y|^2] + \mathbb{E}_{\mathcal{D}_{OOD}}[|c(x)|^2] \leq \varepsilon_{\hat{\mathcal{D}}_{ID}}(h) + \frac{1}{2}d_{\bar{\mathcal{H}}}(\hat{\mathcal{D}}_{ID}, \hat{\mathcal{D}}_{OOD}) + \Delta + \mathcal{O}\left(\sqrt{\frac{d \log(n/d) + \log(1/\delta)}{n}}\right)$$

where  $\bar{\mathcal{H}} := \{\text{sign}(|h(x) - h'(x)| - t)|h, h' \in \mathcal{H}, 0 \leq t \leq 1\}$ .

*Proof.* To present a proof for the first bound (i), likewise Lemma 3 of Zhao et al. (2018), we start to review a triangle inequality for all  $h, h', h'' \in \mathcal{H}$ , for any  $\mathcal{D}$  on  $\mathcal{X}$ , and for error function  $\varepsilon_{\mathcal{D}}(\cdot, \cdot)$ , the inequality  $\varepsilon_{\mathcal{D}}(h, h') \leq \varepsilon_{\mathcal{D}}(h, h'') + \varepsilon_{\mathcal{D}}(h'', h')$  holds. Here, we use  $\varepsilon_{\mathcal{D}}(h, h')$  to denote  $\mathbb{E}_{x \sim \mathcal{D}}[|h(x) - h'(x)|]$ . Now, given  $h^* := \arg \min_{h \in \mathcal{H}} \varepsilon_{\mathcal{D}_{ID}}(h) + \varepsilon_{\mathcal{D}_{OOD}}(h)$  and  $\Delta := \varepsilon_{\mathcal{D}_{ID}}(h^*) + \varepsilon_{\mathcal{D}_{OOD}}(h^*)$ , we have

$$\begin{aligned} \varepsilon_{\mathcal{D}_{OOD}}(h) &\leq \varepsilon_{\mathcal{D}_{OOD}}(h^*) + \varepsilon_{\mathcal{D}_{OOD}}(h, h^*) && \text{(by triangle ineq.)} \\ &= \varepsilon_{\mathcal{D}_{OOD}}(h^*) + \varepsilon_{\mathcal{D}_{OOD}}(h, h^*) - \varepsilon_{\mathcal{D}_{ID}}(h, h^*) + \varepsilon_{\mathcal{D}_{ID}}(h, h^*) \\ &\leq \varepsilon_{\mathcal{D}_{OOD}}(h^*) + |\varepsilon_{\mathcal{D}_{OOD}}(h, h^*) - \varepsilon_{\mathcal{D}_{ID}}(h, h^*)| + \varepsilon_{\mathcal{D}_{ID}}(h, h^*) \\ &\leq \varepsilon_{\mathcal{D}_{OOD}}(h^*) + \varepsilon_{\mathcal{D}_{ID}}(h, h^*) + \frac{1}{2}d_{\bar{\mathcal{H}}}(\mathcal{D}_{ID}, \mathcal{D}_{OOD}) && \text{(by Lemma. 1 of Zhao et al. (2018))} \\ &\leq \varepsilon_{\mathcal{D}_{OOD}}(h^*) + \varepsilon_{\mathcal{D}_{ID}}(h) + \varepsilon_{\mathcal{D}_{ID}}(h^*) + \frac{1}{2}d_{\bar{\mathcal{H}}}(\mathcal{D}_{ID}, \mathcal{D}_{OOD}) && \text{(by triangle ineq.)} \\ &= \varepsilon_{\mathcal{D}_{ID}}(h) + \frac{1}{2}d_{\bar{\mathcal{H}}}(\mathcal{D}_{ID}, \mathcal{D}_{OOD}) + \Delta && (3) \end{aligned}$$

where  $\varepsilon_{\mathcal{D}}(h)$  is defined as  $\varepsilon_{\mathcal{D}}(h) := \mathbb{E}_{x \sim \mathcal{D}}[|h_0(x) - h(x)|]$  and  $h_0(\cdot) := \arg \min_{h \in \mathcal{H}} \mathbb{E}_x[|h(x) - \mathbb{E}_y[y|h(x)]|^2]$  denotes a desired calibrated predictor for label  $y$ .

The above bound is defined over the true population distribution  $\mathcal{D}_{\text{ID}}$  and  $\mathcal{D}_{\text{OOD}}$ . For the ID domain, we can confine our analysis to empirical distribution  $\hat{\mathcal{D}}_{\text{ID}}$  with  $n$  i.i.d. samples generated from  $\mathcal{D}_{\text{ID}}$ , by leveraging a generalization bound on a single domain regression setting (Mohri et al., 2018; Zhao et al., 2018). If  $\mathcal{P}dim(\mathcal{H}) = d$ , for all  $h \in \mathcal{H}$ , below bound holds with probability at least  $1 - \delta$ .

$$\varepsilon_{\mathcal{D}_{\text{OOD}}}(h) \leq \varepsilon_{\hat{\mathcal{D}}_{\text{ID}}}(h) + \frac{1}{2}d_{\bar{\mathcal{H}}}(\mathcal{D}_{\text{ID}}, \mathcal{D}_{\text{OOD}}) + \Delta + \mathcal{O}\left(\sqrt{\frac{d \log(n/d) + \log(1/\delta)}{n}}\right) \quad (4)$$

Then, the true  $d_{\bar{\mathcal{H}}}(\mathcal{D}_{\text{ID}}, \mathcal{D}_{\text{OOD}})$  can also be bounded (with probability at least  $1 - \delta$ ) by an empirical estimator of it as below (See Section 4; Lemma 1 of Ben-David et al. (2010)):

$$d_{\bar{\mathcal{H}}}(\mathcal{D}_{\text{ID}}, \mathcal{D}_{\text{OOD}}) \leq d_{\bar{\mathcal{H}}}(\hat{\mathcal{D}}_{\text{ID}}, \hat{\mathcal{D}}_{\text{OOD}}) + \mathcal{O}\left(\sqrt{\frac{d \log(n/d) + \log(1/\delta)}{n}}\right) \quad (5)$$

By incorporating the inequality 4 and 5 into inequality 3, we complete part (i) of Theorem 3.

$$\varepsilon_{\mathcal{D}_{\text{OOD}}}(h) \leq \varepsilon_{\mathcal{D}_{\text{ID}}}(h) + \frac{1}{2}d_{\bar{\mathcal{H}}}(\hat{\mathcal{D}}_{\text{ID}}, \hat{\mathcal{D}}_{\text{OOD}}) + \Delta + \mathcal{O}\left(\sqrt{\frac{d \log(n/d) + \log(1/\delta)}{n}}\right) \quad (6)$$

Next, we provide a proof for the second part of Theorem 3 that is based on the decomposition of mean-squared classification error (Murphy, 1972) as below:

$$\underbrace{\mathbb{E}[|h(x) - y|^2]}_{\text{classification error}} = \underbrace{\mathbb{E}[|h(x) - c(x)|^2]}_{\text{calibration error}} + 1 - \underbrace{\mathbb{E}[|c(x)|^2]}_{\text{sharpness}} \quad (7)$$

where  $h(\cdot) : \mathcal{X} \rightarrow [0, 1]$ ,  $c(x) := \mathbb{E}_y[y|h(x)]$ , and  $y \in \{0, 1\}$ . Note that, by definition of  $\varepsilon_{\mathcal{D}}(h) = \mathbb{E}_{x \sim \mathcal{D}}[|h_0(x) - h(x)|]$  and  $h_0(\cdot) = \arg \min_{h \in \mathcal{H}} \mathbb{E}_x[|h(x) - c(x)|^2]$ , we can directly plug the equation D into the calibration error bound (inequality D) to obtain below:

$$\mathbb{E}_{\mathcal{D}_{\text{OOD}}} [|h(x) - y|^2] + \mathbb{E}_{\mathcal{D}_{\text{OOD}}} [|c(x)|^2] \leq \varepsilon_{\mathcal{D}_{\text{ID}}}(h) + \frac{1}{2}d_{\bar{\mathcal{H}}}(\hat{\mathcal{D}}_{\text{ID}}, \hat{\mathcal{D}}_{\text{OOD}}) + \Delta + \mathcal{O}\left(\sqrt{\frac{d \log(n/d) + \log(1/\delta)}{n}}\right)$$

□